Two-Dimensional and Three-Dimensional Seismic Surveys: The Potential for Imaging the Shallow Subsurface at a Carbon Dioxide Geological Storage Site

S. Yordkayhun* and C. Juhlin**
**Department of Physics, Faculty of Science, Prince of Songkla University, Hatyai, Songkhla, 90112, Thailand*
***Department of Earth Sciences, Uppsala University, Villavagen 16, 75236, Uppsala, Sweden*

ABSTRACT

Conventional seismic methods that focus on investigating deep formations have relatively sparse distribution of source and receiver positions, thus limiting frequency content of the data and artifacts of the processing. This results in the upper part of seismic images being poorly resolved. In order to fill this information gap, imaging the shallow subsurface using seismic travel time inversion, travel time tomography, and seismic reflection techniques was the goal of this study. Two-dimensional and three-dimensional data acquired in conjunction with site characterization and monitoring aspects at a carbon dioxide geological storage site at Ketzin, Germany, were used for this study. For this data set, the ability to obtain high-quality images was limited by source-generated noise and time shifts due to near-surface effects that produced severe data distortions. These time shifts were comparable to the dominant periods of the reflections and to the size of structures to be imaged. Therefore, a combination of seismic refraction and state-of-the-art processing techniques resulted in key image improvements and allowed new information to be extracted. The results from these studies, together with borehole information and hydrogeologic information, were combined into an integrated interpretation. The uppermost reflecting horizon, the boundary between the Quaternary and Tertiary units, and shallow structures associated with the shallow aquifer/aquitard complex and the major fault zones were mapped. Some of the major faults appear to project into the Tertiary unit. These findings are important for understanding the potentially risky areas and can be used as a database for the future monitoring program at the site.

KEYWORDS: Inversion, travel time tomography, three-dimensional seismic surveys, seismic velocity, carbon dioxide geological storage, global warming

INTRODUCTION

By prediction from statistical analysis, mankind faces significant climate change by the end of this century as a result of continuing global warming (IPCC, 2007; Bachu, 2008). It is generally accepted that the main cause of the observed global warming is the increase in atmospheric concentrations of

greenhouse gases. In particular, increasing consumption of fossil energy resources is the main factor for the increase of carbon dioxide concentration, the most important gas responsible for the greenhouse effect. Consequently, the development of greenhouse gas mitigation technologies plays an important role as a potential response to global warming. Carbon dioxide capture and storage is becoming an increasingly important concept in this respect (Gale, 2004; IPCC, 2005; Wildenborg and Lokhorst, 2005). The principle is: capture carbon dioxide from large sources instead of releasing it into the atmosphere, transport it to a storage site, and inject it at depths of at least several hundreds of meters.

A pilot scale carbon dioxide geological storage project, CO_2SINK, is being carried out to clarify and establish the technology for storage and later monitoring of carbon dioxide generated from large-scale emission sources. The site is located in Ketzin in northern Germany. Determining the geometry of the storage formation and overlying units, monitoring the movement of carbon dioxide, and the physical and chemical changes within the storage formation when carbon dioxide is injected are important aspects of any research program on geological storage of carbon dioxide. A number of studies have shown that three-dimensional seismic monitoring plays an important role in these issues (Arts and others, 2006).

Figure 1 shows the location of the data sets discussed in the study. The main focus has been to study in detail the crest of the anticline. However, two-dimensional seismic lines further east were initially studied. A pilot two-dimensional seismic reflection survey was acquired as preparatory work before carrying out the three-dimensional baseline seismic survey at the Ketzin site. Results of the two-dimensional and three-dimensional seismic processing show that the deeper part of the subsurface was clearly imaged, but some details were lost in the uppermost part due to resolution limits, acquisition geometry, and processing artifacts. Consequently, focus was put on the application of high resolution seismic techniques by integrating seismic reflection and seismic refraction methods to study the potential for improving the image of the upper 400 meter of the subsurface. This depth range hosts cap rock, shallow faults, an aquifer system, and the abandoned natural gas storage formations. Thus, characterizing the shallow subsurface is important in terms of site delineation of potential leakage paths and monitoring and risk assessment after carbon dioxide has been injected. Due to the complicated nature of the near-surface environment, high resolution is required to obtain detailed images. However, for the depth of interest, interference between source-generated noise and shallow reflections, near-surface effects, and time shifts are challenges. Especially, time shifts are comparable to the dominant periods of the reflections and to the size of the target structures. This limits the degree to which the shallow structures may be imaged. Therefore, the main effort was to optimize the application of high resolution seismic techniques and reconstruct the near-surface model with greater accuracy and higher resolution in order to fill the gap between the deep and shallow parts of the subsurface. In this study, results from the reprocessed subset of the three-dimensional seismic data,

together with shallow borehole information, the two-dimensional shallow velocity-depth model, and the three-dimensional tomography study, were combined into an integrated interpretation.

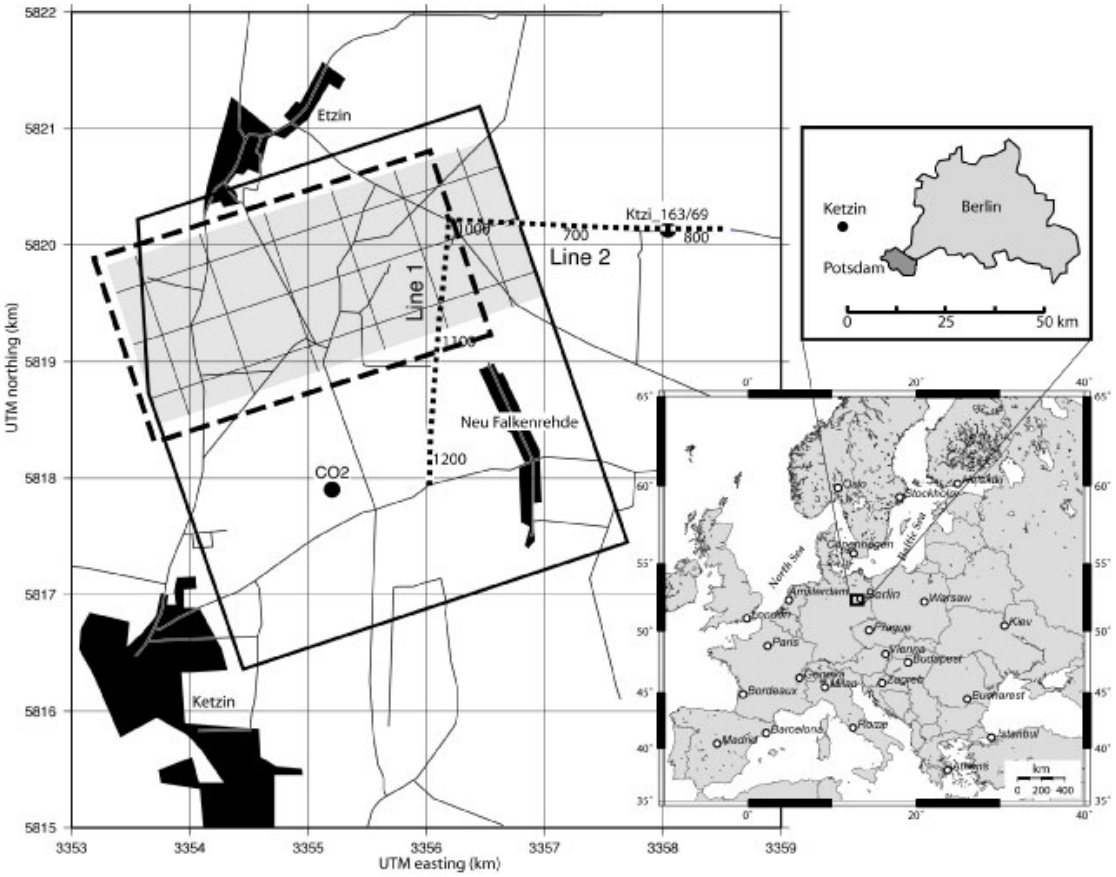

Figure 1. Map of the Ketzin study area west of Berlin, Germany. The area marked by the polygon approximately encloses the area for the main 3D survey. The two 2D pilot profiles are marked by dotted lines as Line 1 (N-S profile) and Line 2 (E-W profile). Borehole Ktzi 163/69 is indicated by the circle. The injection site (CO2) is also indicated. The dashed rectangle encloses the tomography study area. The shaded area with grid lines highlights the 3D seismic surface coverage area discussed in this study.

SITE GEOLOGY AND HYDROGEOLOGY

The Ketzin site is located in part of the Permian basin system of the northeast German basin. The injection site is situated on the eastern part of a north northeast-south southwest-trending double salt anticline, with flanks that gently dip about 15 degrees (Förster and others, 2006), consisting of a sequence of mainly sandstone, siltstone, and mudstone.

Quaternary sediments form local hills with relief as great as 30 meters. The thickness of these sediments is 50 to 80 meters. This Quaternary unit, together with sandy Tertiary deposits, hosts the main freshwater aquifers in the area. Below these deposits, the Tertiary Rupelton clay, with a thickness

of 80 to 90 meters, acts as a major aquitard and separates the saline waters of the deeper aquifers from the upper fresh water reservoir. The Quaternary-Tertiary groundwater system consists of three main aquifers, L3 to L1, and several aquitards (Figure 2). At the western and eastern flanks of the Ketzin anticline, deep north northeast-south southwest-oriented Quaternary incision troughs cut the Rupelton clay. Here, the Quaternary sediments are up to 300 meters thick and additional deep Quaternary aquifers are present, L4 in Figure 2 (Manhenke, 2002).

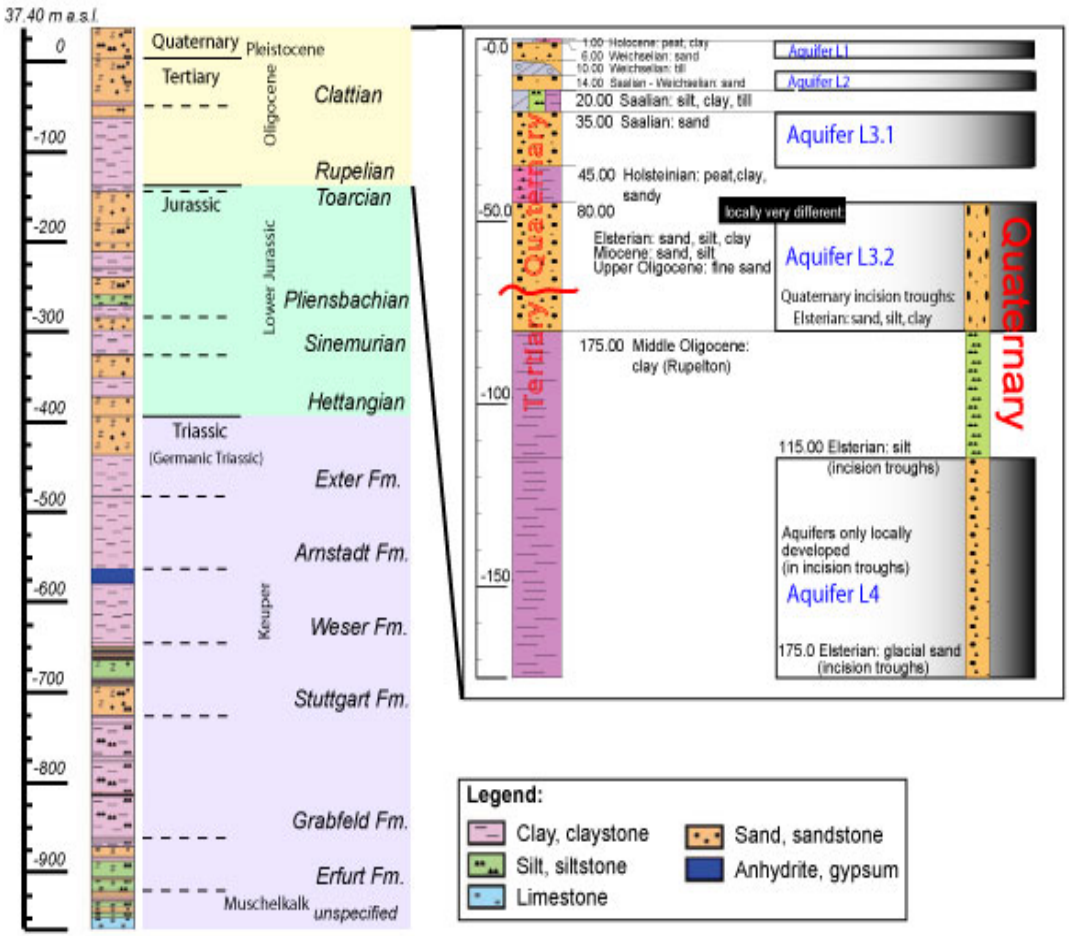

Figure 2. Geological structures of the site inferred from a local borehole in Ketzin and adjacent boreholes (modified after *Förster et al*., 2006 and *Juhlin et al*., 2007). Schematic hydrogeological profile of the study area showing the main aquifers and aquitards of the prae-Rupelian groundwater system. Aquifer numbers are used according to *Manhenke*, 2002.

The Rupelton clay acted as the effective cap rock for the natural gas that was stored in the underlying Jurassic sandstone until the year 2000. These Jurassic sandstone beds, at depths between 250 meters and 400 meters, together with interbedded mudstone and siltstone, form a saline multi-aquifer system.

Deeper down, Upper Triassic playa-type rocks of the Weser and Arnstadt Formations, composed mainly of mudstone, dolomitic to anhydritic mudstone, and anhydrite, form an approximately 160-meter thick cap rock section above the Stuttgart Formation (Förster and others, 2006). An approximately 20-meter thick anhydrite layer within this section occurs at the top of the Weser Formation. It is known as the K2 reflector and has been identified on vintage seismic data and in the baseline three-dimensional seismic volume (Juhlin and others, 2007). It occurs at depths of 500 to 700 meters below sea level and about 80 meters above the top of the Stuttgart Formation at the CO_2SINK injection site. The sandstone beds of the lithologically very heterogeneous Stuttgart Formation, a thickness of 70 to 80 meters, are the target reservoir for the carbon dioxide injection at Ketzin.

DATA ACQUISITION

Two-Dimensional Data

The pilot reflection seismic data were acquired in September, 2004. Two perpendicular lines, running mostly along two agricultural roads near the target area of the planned three-dimensional survey, were acquired (Figure 1). Line 1 was a traditional agricultural road, while line 2 was hard soil that had been compressed by heavy military equipment. The pilot study consisted of testing both source and receiver performance. Three different sources, VIBSIST, weight drop, and Minivib were tested along the two lines. The measurements were carried out according to the same scheme for every source. Initially, tests and parameter tuning were done at five selected locations on, or close to, line 2. Data were acquired by shooting at all stations on both profiles, allowing common mid-point stacked sections to be produced. Source and receiver spacing was 20 meters. Data were recorded on 240 channels, fixed spread. Sources activated on line 1 were also recorded on line 2, and vice versa, providing the possibility for a pseudo three-dimensional analysis of the survey area. Only a few selected source stations were skipped due to the presence of underground gas lines. The tests also included comparison of 10 hertz and 28 hertz single geophones and 10 hertz geophone arrays on line 2 and a comparison of geophones planted on the surface and in holes 30 to 40 centimeters deep.

Three-Dimensional Data

The three-dimensional seismic survey consisted of approximately 12 square kilometers of subsurface coverage and was acquired in autumn 2005. The acquisition pattern was a template scheme. Each template contained five parallel in-line direction receiver lines spaced 96 meters apart. Each line had 48 single 28 hertz geophones at 24-meter intervals. For each deployment of the receiver pattern in a template, eight to nine hits per station by a weight drop source were shot regularly at 24-meter and 72-meter intervals along 12 lines perpendicular to the cross-line direction of receiver lines and were

spaced 48 meters apart, giving roughly 200 shot locations per template. The template was shifted along the in-line and cross-line directions between swaths in a snaking manner and half the template was kept in place when shifting to the next template. The resulting overlap between the templates gave an even nominal fold of 25 with a 12-meter by 12-meter common mid-point bin size and a good distribution of azimuths versus offset. However, due to the logistics, lower fold data were recorded in some areas.

METHODOLOGY

To study the potential of imaging the shallow subsurface, three seismic techniques were performed.

First Arrival Travel Time Inversion by Generalized Linear Inversion Methods

Picked first arrival travel times from shots by the weight drop source from the pilot two-dimensional reflection seismic data were used as input in this study and stacked sections were compared in interpreting the resulting velocity-depth models. The first arrival travel time inversion technique, generalized linear inversion proposed by Hampson and Russell (1984), was used for generating the velocity-depth model. It is based on ray tracing through a best-guess initial velocity model and solving the problem of optimizing the fit of the calculated to observe travel times in a least-squares sense (Menke, 1984). The model update procedure for either depth or velocity consists of a looping process that is similar to that used in tomographic inversion. The method is composed of:

1. Setting up an initial velocity model using a decimated set of picked travel times for velocity control points.

2. Theoretical first arrival travel times are calculated by the ray tracing method from each shot-receiver pair.

3. The travel time residuals, or errors, the difference between the picked first arrival times and the theoretical first arrival times, are calculated.

4. The generalized linear inversion algorithm solves the equation by linearizing it in the vicinity of the initial guess and updating the thickness and velocities of the layers. This procedure is repeated until some acceptable correspondence is reached between observed and computed first break picks.

5. The difference of the resulting model relative to the real complex earth model can be treated as a set of residual surface-consistent time shifts, or short-wavelength static or time residuals. In order to recover the high frequency anomalies present in the original first breaks that may be missing from the final model, the short-wavelength time residuals are calculated and applied after the final iteration.

Three-Dimensional Travel Time Tomography

Three-dimensional seismic travel time tomography was applied to a subset of three-dimensional data, covering an area at the crest of anticline. In seismic travel time tomography, an unknown velocity model is inferred from the observed arrival times of seismic waves. This relationship is given by the path integral for the travel time, *t*, for one source-receiver pair:

$$t = \int_{l\{s(r)\}} s(r)dl \tag{1}$$

where *s(r)* is the slowness, *dl* is the differential length, and *l(s)* represents the raypath which is a function of *s(r)*. This is a non-linear problem in the sense that the seismic ray bending depends on the unknown velocity structure. A standard technique for dealing with this is to linearize the travel time equation about some initial, or reference model (Benz and others, 1996). In the algorithm used, PStomo_eq (Tryggvason and others, 2002), the forward calculation of travel times in the model is done on a uniform grid by solving a first-order finite-difference approximation of the eikonal equation (Podvin and Lecomte**,** 1991; Tryggvason and Bergman, 2006). Once the travel times to all receivers are known, the raypaths are found by ray tracing backward from the receiver locations perpendicular to the isochrones (Vidale, 1988). The updates to the model are solved for iteratively by the least-squares QR conjugate gradient solver (Paige and Saunders, 1982). Bergman and others (2004) found in a high-resolution near-surface application for a till-covered bedrock environment that the travel time delays due to the unconsolidated layer were causing artifacts in the resulting velocity model. To overcome the problem, they suggested a static term should be included in the linearized travel time equation,

$$r_{ij} = t_j + \sum_{n}^{N} \frac{\partial T_{ij}}{\partial u_n} \Delta u_n, \quad i = 1,...,I, \quad j = 1,...,J \tag{2}$$

where r_{ij} is the travel time residual between source *i* and receiver *j*, t_j the static shift at receiver *j*, T_{ij} is the travel time between the source and receiver, and Δu_n the slowness perturbations in each cell passed by the ray. In this study, the tomographic inversion scheme similar to the one of Bergman and others (2006) was performed over five iterations. Each iteration consisted of the following steps:

1. Forward computation of travel times and raypaths.
2. Simultaneous inversion for the velocities and the static shifts.
3. Computed statics distributed between sources and receivers.
4. New statics applied to the data.

This sequence is repeated until a total root mean square data misfit, including the statics, matching the estimated data error is obtained.

Three-Dimensional Seismic Reflection Processing

Data from two swaths located over the fault zone area were extracted from the entire three-dimensional volume and were truncated to a maximum travel time of 400 milliseconds and a maximum offset of 400 meters. Figure 3a shows a typical example of a shot gather. The direct and refracted arrivals and strong reflection events are observed over the offset range used, together with a clear noise cone consisting mainly of ground roll that masks reflections up to 200-meter offset.

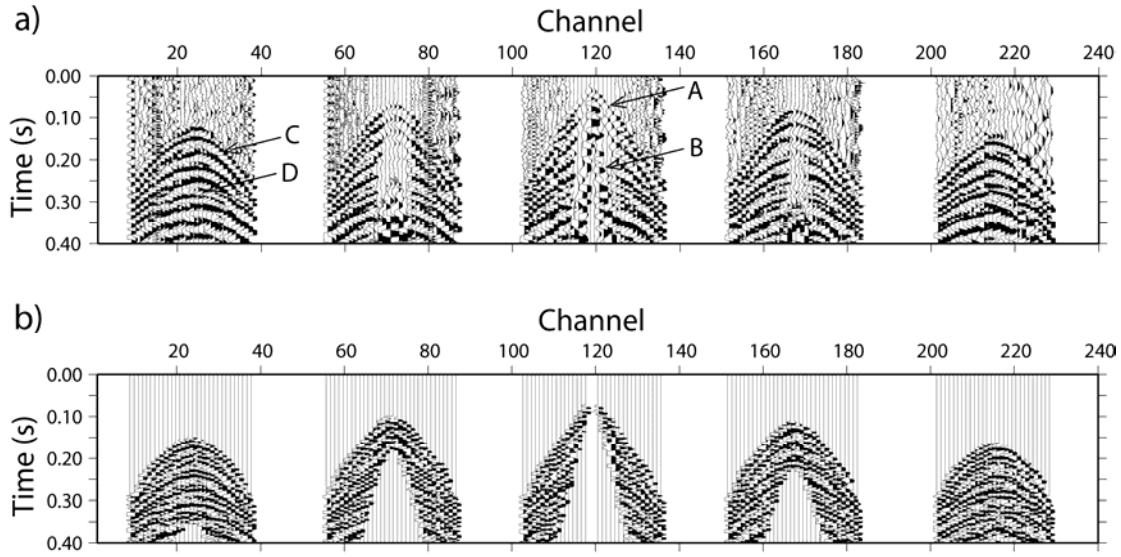

Figure 3. (a) A typical shot gather (shot located in the center of the area). The refracted wave (A), reflected wave (C), diffraction event (D) and strong surface waves/ground roll (B) were observed over the maximum observation offset of 400 m. (b) The processed shot of (a) before stack.

The processing sequence for this data subset is outlined in Table 1. The most important processing steps were:

- More accurate three-dimensional refraction statics recalculated using a near-surface model obtained from all first arrival times picked on all offsets up to 400 meters. The residual moveout was taken into account. Ten percent of the residual moveout with respect to the surface was accounted for by moving the datum 10 meters down from the surface.
- Given the trade-off between common mid-point bin size and frequency content, data were bandpass filtered at 30 to 100 hertz after deconvolution.
- A mute function containing the entire noise cone of ground roll performed best as a tail mute. Carefully designed top mutes were used to eliminate direct and refracted waves from common mid-point gathers and a 100 percent stretch mute was used in the normal moveout correction.

Following the application of pre-stack processing steps, the signal-to-noise ratio and resolution were markedly enhanced, as illustrated by shot gathers in Figure 3b.

- The final velocity function used for normal moveout corrections was updated after the velocity analysis-residual static corrections cycle. This velocity function proved to be appropriate for migration and time-to-depth conversion.
- The coherency enhanced stacked volume was migrated to collapse diffractions and to improve lateral resolution.

RESULTS AND DISCUSSIONS

Two-Dimensional Shallow Velocity-Depth Model

The velocity-depth models for lines 1 and 2 are quite similar, consisting of a sequence of uniform layers, except for the differences in geometry. The velocity-depth models for both profiles are fairly homogeneous laterally and velocity increases slowly with depth.

The depth converted unmigrated sections obtained for lines 1 and 2 using the stacking velocity from the common depth point processing and the velocity-depth models obtained in this study were compared (Figure 4). The depths to the reflections obtained using the generalized linear inversion velocity model are different than the depths obtained using the stacking velocity, implying a discrepancy between the two velocity functions.

In order to compare the generalized linear inversion models directly with the reflection seismic sections, they were superimposed on top of the depth sections (Figure 4). It is obvious that layer boundaries as defined by clear reflections on the seismic sections are more consistent with velocity boundaries from the generalized linear inversion models obtained when using the velocity-depth models from this study compared to using the Dix velocities for depth conversion. This result indicates that use of the generalized linear inversion velocity fields produces a better time-to-depth conversion of the reflection data, at least in the upper 300 meters. However, some reflectors, those within the yellow zone in Figure 4a and 4b, have not been detected in these models. This is probably due to a possible fault zone between position 600 to 1200 meters in line 1 where the rays pass through a complex structure and to generalized linear inversion being solved by a ray-based approach, implying the ray path is biased to high velocity layers whereas the reflections may be due to low velocity zones. Correlation is better between layer boundaries where the reflector is clear, as shown by an arrow marked at about a 350-meter depth in Figure 4b.

Geological interpretation based on the combination of models, the reflection seismic sections, and data from the Ktzi 163/69 borehole shows that the upper 400 meters of the subsurface are represented by four groups of sediments. In general, the uppermost layer consists of low velocity, 1000 meters per second, unconsolidated sediments that have a thickness varying from 5 meters, where topography is

fairly flat, to 15 to 30 meters, where topographic relief is high. Quaternary sandstone deposits with velocities of 1600 to 1700 meters per second and 50 to 110 meters thick occur below these unconsolidated sediments. The velocities suggest saturated soil material in a shallow aquifer as the composition of this layer. This unit is underlain by Tertiary deposits of mudstone with velocities of 1950 to 2050 meters per second and thickness ranging from 60 to 120 meters. Below this Tertiary unit, Jurassic sedimentary sequences are represented by an alternating sequence of sandstone, mudstone, and siltstone that extends to depths of about 250 to 400 meters and has velocities in the range of 2300 to 2600 meters per second.

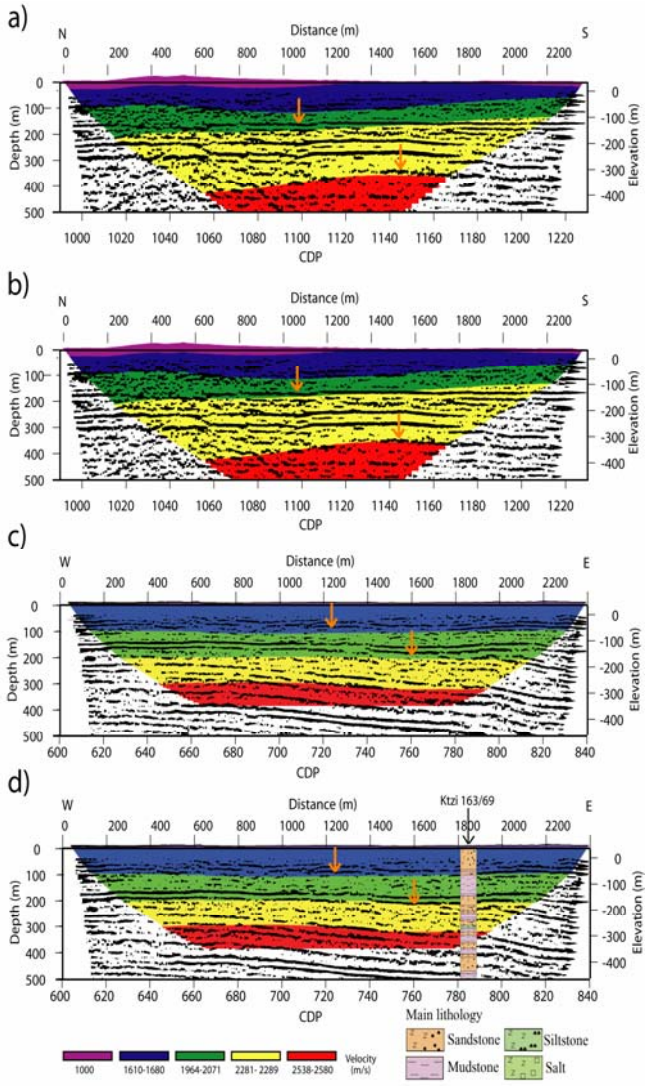

Figure 4. Depth section overlain by the GLI model of Line 1 (a and b) and Line 2 (c and d) using the Dix velocity (top) and the GLI velocity (bottom). Orange arrows mark examples of locations where the correlation between the depth section and the GLI model is better than with the Dix velocities. Geologic interpretation is constrained by information from the Ktzi 169/63 borehole.

Tomographic Images

Boreholes located near each profile in Figure 5 allow for direct comparison of the velocity model with lithological boundaries. The images show several coherent structures along the profiles. The low velocity, 800 to 1200 meters per second, near-surface layers represent the uppermost unconsolidated material consisting mostly of sand. The thickness of this layer varies from near zero up to 20 meters in regions of high topography. The boundary between the Quaternary unit and the Tertiary clay unit, which was not mapped in the seismic reflection volume in Juhlin and others (2007), is identified on the basis of where the velocity reaches approximately 1800 meters per second at a depth of approximately 60 to 80 meters below the surface (Figure 5). Although this boundary does not correlate one to one with borehole observations, the general trend of the transition correlates. Velocities in the range of 1600 to 1800 meters per second probably represent variations in the internal structure of the Quaternary unit and may indicate changes in its aquifer properties. The higher velocities, greater than 1800 meters per second, at some locations in the upper part of this unit are interpreted to reflect the local occurrences of glacial till. This till may act as aquitards within the main aquifer of this unit.

Significant lateral velocity variations are also present in the Tertiary clay unit. These variations are above 1800 meters per second and occur below a depth of 50 meters. Possible reasons for these lateral velocity variations include lateral variations of lithology within the unit, deeper faults extending into the unit, alteration within the unit due to fluid/gas migration along more deep-seated faults, and artifacts from the tomography. Therefore, it is possible that the low velocities in the Rupelton clay may be due to alteration associated with the fault zones, even if the fault zones do not extend into the unit. Support for this interpretation is that these low velocity zones roughly coincide in the model with the extrapolation of the fault zones interpreted in the three-dimensional reflection seismic volume, which are indicated by arrows in Figure 5.

In order to emphasize the fault zones and their possible extension into the near surface, the fault trends from seismic amplitude analysis near the base Tertiary were compared with these results. In the tomography depth slices at 45 to 80 meters, these being 85 to 130 meters below the surface, some of the fault zones can be associated with low velocity anomalies striking mainly east-west (Figure 6). Anomalies A1 and A2 mark possible extensions of the deeper mapped faults into the Tertiary Rupelton clay, whereas anomaly A3 marks a possible altered rock volume associated with other fault zones. Of the three anomalies, A1 correlates most clearly with a mapped fault and can be traced consistently to different depth slices within the Tertiary unit (Figure 6).

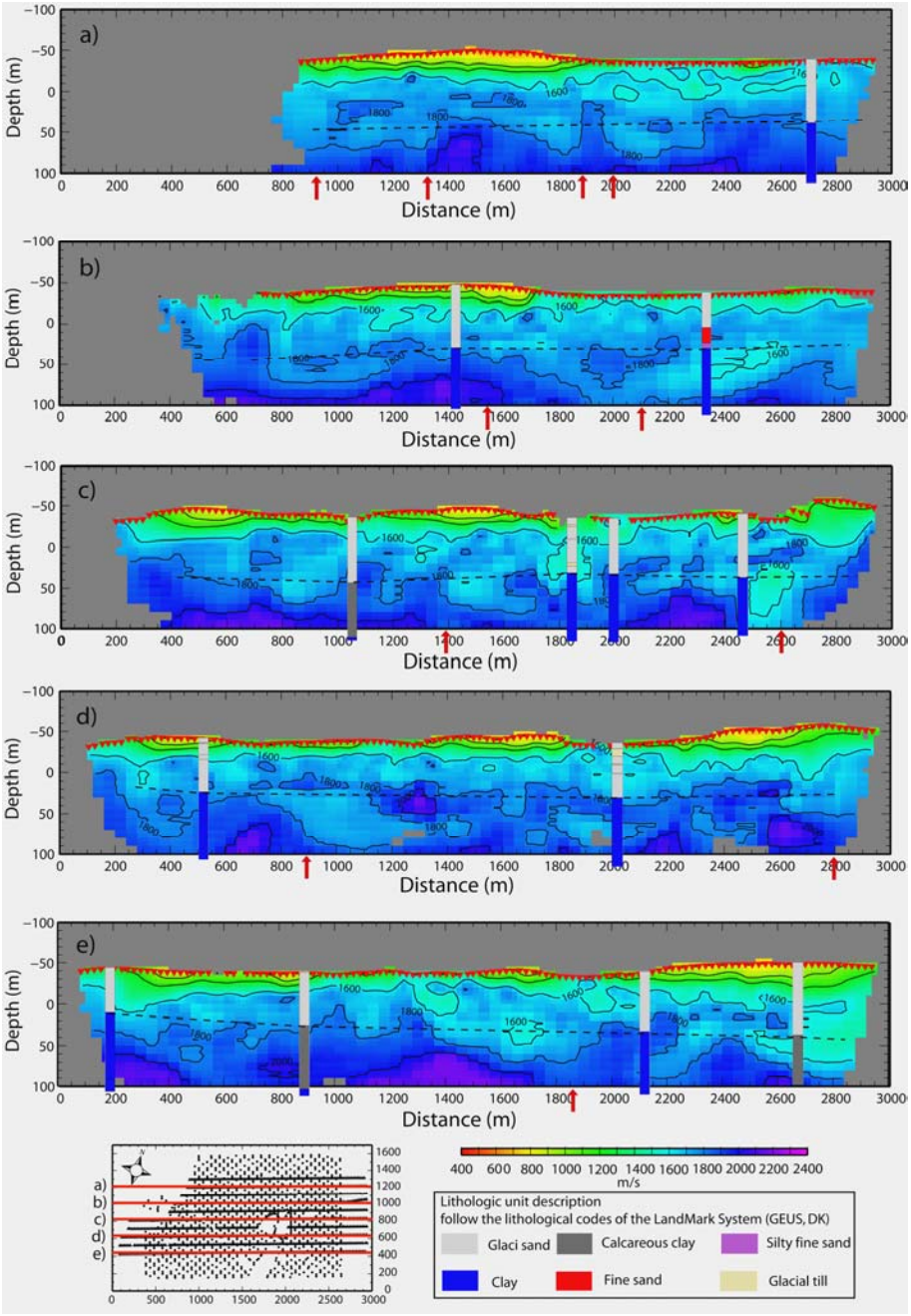

Figure 5. West-east oriented tomographic cross sections (vertical slices) overlain by geological data from nearby boreholes. Locations of the cross sections are shown on the index map. Regions undersampled by the rays are masked. Arrows indicate locations of interpreted faults below the Tertiary unit based on similarity attribute maps of the 3D reflection seismic volume (after Kazemeini and others., 2008). Dashed line highlights the possible Quaternary/Tertiary boundary. Depth is measured relative to sea level and vertical exaggeration is 3:1.

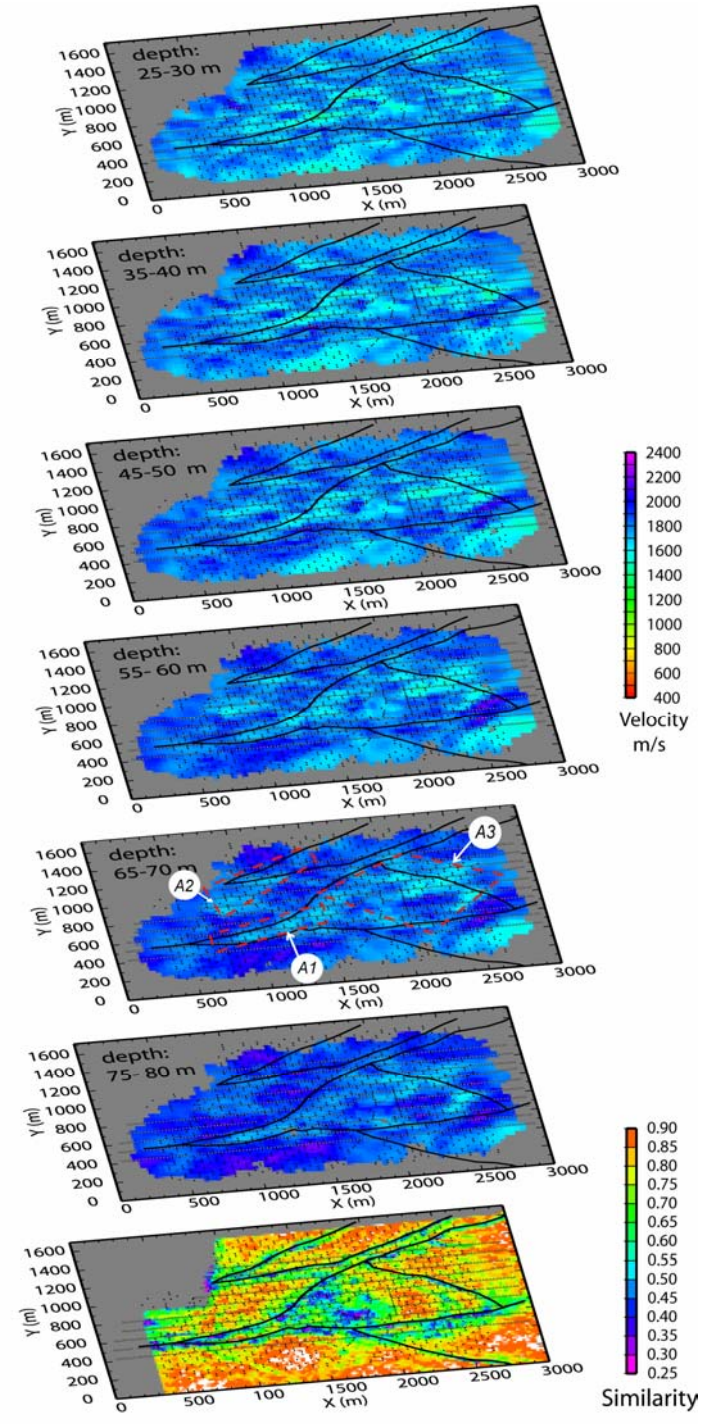

Figure 6. Tomographic depth slices at selected depths. Bottom slice shows similarity attribute map at 150 ms (after Kazemeini and others, 2008). The clear near-linear features in the similarity map are interpreted as representing fault zones and their general geometry are shown as solid lines in the figure. Shots and receivers are marked by dots and triangles, respectively. The regions undersampled by ray paths are masked. A1, A2 and A3 show the location of low velocity anomalies that are discussed in the text.

Seismic Volume and Potential for Near-Surface Faulting

The integration of a sequence of time slices, in-lines and cross-lines from the migrated three-dimensional volume, shallow borehole information, tomographic images, and hydrogeologic information allows structures to be identified reliably in the upper 300 milliseconds. The main reflecting boundaries were mapped semi-automatically on the basis of their characteristic seismic response. These include the near base of the Quaternary, near base of the Tertiary, which was defined as T1 horizon by Reinhardt (1993), near top of the Sinemurian, and the upper and lower gas layers (Figure 7).

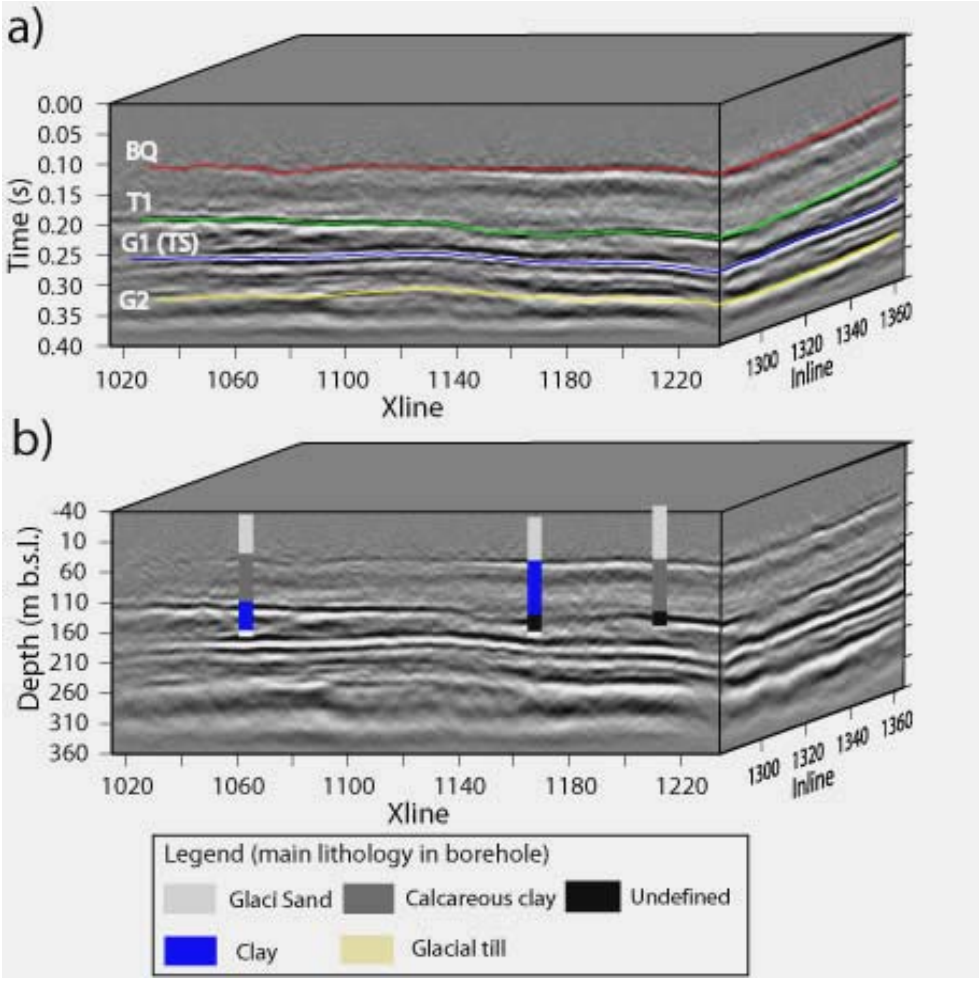

Figure 7. (a) Seismic time volume with picked horizons displayed. BQ = near base Quaternary, T1 = near Base Tertiary, TS = near Top Sinemurian, G1, G2 = the upper, lower gas layers. (b) Seismic depth volume and correlation with boreholes.

The topmost horizon, which is the estimated boundary between Quaternary sediments and the Tertiary clay unit, now occurs at 95 to 120 milliseconds. Correlation between shallow boreholes and the migrated depth volume confirms the presence of this boundary at depths of 65 to 90 meters (Figure 7). The vertical resolution is about 4 to 7 meters and the horizontal resolution after migration is 13.5 meters, which is nearly equivalent to the bin size of 12 meters.

The near base Tertiary is characterized by strong continuous reflections at 200 to 220 milliseconds, this being depths of approximately 150 to 170 meters. Discontinuous portions of this event with lower reflectivity may be associated with collapse or altered rock due to faulting.

Tracking faults to the surface provides better insight on the connection between deeper formations and the near-surface environment and has to be considered for carbon dioxide storage and monitoring issues because faults may also enable shallow secondary accumulations of carbon dioxide to form (IPCC, 2005; Pruess, 2008). In the previous processing (Juhlin and others, 2007), it was generally not clear if the deeper faults imaged on the three-dimensional seismic survey extend to shallower levels than the base of the Tertiary, although the tomographic study indicates that at least one of them might. Therefore, an extensive fault analysis study was made to increase the confidence level of mapping the deeper faults to levels shallower than the base Tertiary.

The fault detection technique used was a neural network multi-attribute analysis based on the interpreter's knowledge (Tingdahl and others, 2001; Meldahl and others, 2001; Tingdahl and de Rooij, 2005). In general, the major fault zones in the area are characterized by prominent east-west to south southwest-trending linear structures on the time slices and fault probability slices (Figure 8). All faults appear to continue up to the base of the Tertiary, this being the 210-millisecond slice. Further up, three fault systems appear to continue into the Tertiary clay unit. Their apparent extension into the clay unit exceeds the vertical resolution limit for the two faults located in the western part of the area. Supporting evidence for the presence of these faults in the Tertiary clay is found in the tomographic images. For example, the tomographic slice at 65 to 70 meters below sea level (Figure 7) shows low velocity anomalous regions that closely coincide with the potential faults mapped in the fault probability slice. In summary, the fault probability analysis shows that at least certain faults may extend across the Tertiary base and can be traced 10 to 30 milliseconds, this being 8 to 25 meters, into the clay unit.

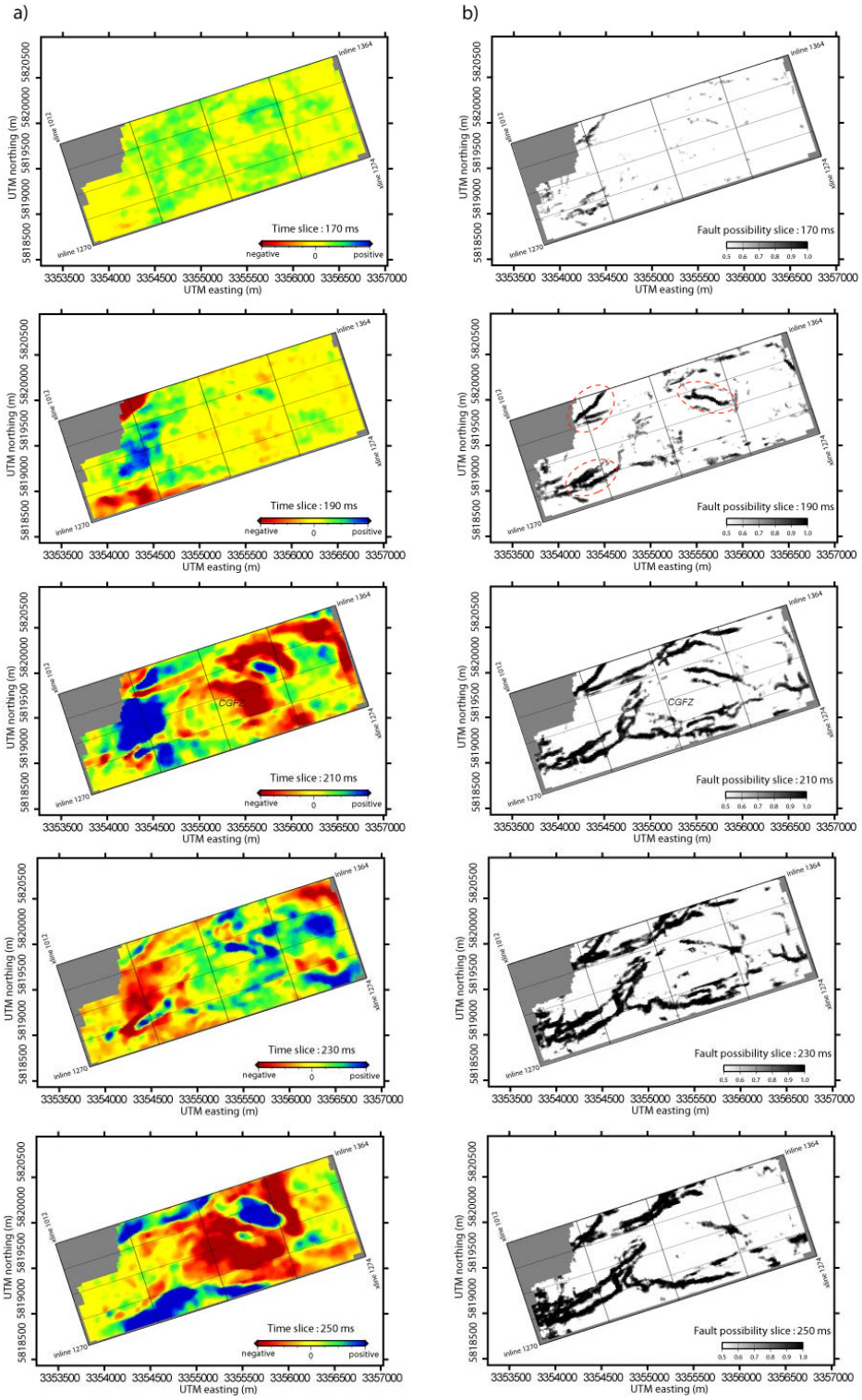

Figure 8. (a) Time slices from 170 ms to 250 ms. (b) Fault probability slices from 170 ms to 250 ms. Faults are characterized in terms of probability with respect to the grey shaded area in the figure. CGFZ denotes the Central Graben Fault Zone. Ellipses mark locations where the faults may extend into the Rupelton clay unit.

CONCLUSIONS

The principal objective of this study was to obtain shallow subsurface information at the CO_2SINK project site in Ketzin, Germany. A number of comprehensive studies were made using two-dimensional seismic data acquired for purposes of acquisition parameter testing and three-dimensional seismic data acquired for purposes of site characterizing and monitoring. The studies focused on:

- Generating the velocity model for the upper 400 meters of the subsurface.
- Characterizing the internal structures of the Quaternary and Tertiary units.
- Mapping the boundary between Quaternary and Tertiary units.
- Tracking fault projections towards the surface.

Potentially risky areas, including the shallow aquifer, the fault zones at the crest of the anticlinal structure, and the abandoned natural gas storage, are key regions in this study.

Despite the limitations of acquisition geometry and source frequency content, more detailed images on shallow structures were obtained through travel time inversion, travel time tomography, and intensive processing of reflection data.

The first arrival travel time inversion technique provided the velocity-depth model of the subsurface in the upper 400 meters, which represents sedimentary units that are characterized by a gradual increase in velocity with depth and with lateral velocity variations being insignificant. The pilot study lines lie east of the top of the anticline. Lateral variations appear to be less there, perhaps due to less faulting and/or the limitation of the inversion algorithm. Although reliable interpretations were limited by the nature of the refraction-based method, the non-unique solutions of the inversion algorithm, and the highly heterogeneous layers, a more accurate velocity function for time-to-depth conversion of the upper 300 milliseconds of the seismic sections and statics information were obtained.

Three-dimensional travel time tomography, including static correction terms, has imaged the subsurface velocity structures down to a depth of 150 meters. These structures are associated with the main aquifer/aquitard complex system of the Quaternary and the upper part of the Tertiary unit. Some of the fault zones may extend into the Tertiary section. Although reliable and robust models were obtained, interpretation on the fault projection-related anomalies and the boundary between the Quaternary and Tertiary in the tomographic image remain subjective due to the limitation of tomography resolution in the deeper parts, the bias of raypaths, and the effect of rock alteration over fault zones.

In an attempt to constrain and further improve these images, the processing parameters for imaging the shallow structures were optimized on a subset of the three-dimensional seismic reflection data. The boundary between the Quaternary and Tertiary units was recovered and is consistent with the

boundary encountered in the boreholes. An intensive fault analysis study indicates possible projection of faults further into the Tertiary unit and adds support to the tomography results.

ACKNOWLEDGEMENTS

The CO_2SINK project is financed by the EU commission, the German Federal Ministry of Education and Research, the German Federal Ministry of Economics and Technology, research institutes, and industry under project No. 502599. We thank the project coordinator, GeoForschungsZentum Potsdam, for providing supplementary data sets.

REFERENCES

Bachu, S. 2008. CO_2 storage in geological media: Role, means, status and barriers to deployment. *Progress in Energy and Combustion Science* **34**, 254–273.

Benz, H.M., Chouet, B.A., Dawson, P.B., Lahr, J.C., Page, R.A. and Hole, J.A. 1996. Three-dimension P and S wave velocity structure of Redoubt Volcano, Alaska. *Journal of Geophysical Research* **101**, 8111-8128.

Bergman, B., Tryggvason, A. and Juhlin, C. 2004. High-resolution seismic tomography incorporating static corrections applied to a till covered bedrock environment. *Geophysics* **69**, 1082–1090.

Bergman, B., Tryggvason, A. and Juhlin, C. 2006. Seismic tomography studies of cover thickness and near-surface bedrock velocities. *Geophysics* **71**, U77–U84.

Förster, A., Norden, B., Zinck-Jørgensen, K., Frykman, P., Kulenkampff, J., Spangenberg, E., Erzinger, J., Zimmer, M., Kopp, J., Borm, G., Juhlin, C., Cosma, C. and Hurter, S. 2006. Baseline characterization of the CO_2SINK geological storage site at Ketzin, Germany. *Environmental Geosciences* **13**, 145-161.

Gale, J. 2004. Geological storage of CO_2: What do we know, where are the gaps and what more needs to be done?. *Energy* **29**, 1329-1338.

Hampson, D. and Russell, B. 1984. First-break interpretation using generalized linear inversion. *Journal of the Canadian Society of Exploration Geophysicists* **20**, 40-54.

Intergovernmental Panel on Climate Change (IPCC). 2005. In: Special report on carbon dioxide capture and storage (Metz, B., Davidson, O., de Coninck, H.C., Loos, M. and Mayer, L.A.,) Cambridge University Press, Cambridge, UK

IPCC (Intergovernmental panel on climate change). 2007. Climate change 2007: The physical science basis. Fourth assessment report, IPCC Secretariat, Geneva, Switzerland.

Juhlin, C., Giese, R., Zinck-Jørgensen, K., Cosma, C., Kazemeini, H., Juhojuntti, N., Lüth, S., Norden, B. and Förster, A. 2007. 3D baseline seismics at Ketzin, Germany: The CO_2SINK project. *Geophysics* **72**, B121-B132.

Kazemeini, H., Juhlin, C., Zinck-Jørgensen, K. and Norden, B. 2008. Application of the continuous wavelet transform on seismic data for mapping of channel deposits and gas detection at the CO_2SINK site, Ketzin, Germany. *Geophysical Prospecting*, DOI: 10.1111/j.1365-2478.2008.00723.x.

Manhenke, V. 2002. Hydrostratigraphische Gliederung der känozoischen Lockergesteine von Brandenburg (in German), Brandenburgische Geowiss. Beitr., 9, 1/2, 59-64.

Meldahl, P., Heggland, R., Bril, A.H. and de Groot, P.F. 2001. Identifying targets like faults and chimneys using multi-attributes and neural networks. *The Leading Edge* **20**, 474–482.

Menke, W. 1984. Geophysical data analysis: Discrete inverse theory. Academic Press Inc., New York, 289 pp.

Paige, C.C. and Saunders, M.A. 1982. An algorithm for sparse linear equations and sparse least squares. *ACM Transactions on Mathematical Software* **8**, 43-71.

Podvin, P. and Lecomte, I. 1991. Finite different computation of travel times in very contrasted velocity models: A massively parallel approach and its asscociated tools. *Geophysical Journal International* **105**, 271-284.

Pruess, K. 2008. Leakage of CO_2 from geologic storage: Role of secondary accumulation at shallow depth. *International Journal of Greenhouse Gas Control* **2**, 37-46.

Reinhardt, H.G. 1993. Regionales Kartenwerk der Reflexionsseismik. *VEB Geophysik Leipzig*.

Tingdahl, K.M., Bril, A.H. and de Groot, P.F. 2001. Improving seismic chimney detection using directional attributes. *Journal of Petroleum Science and Engineering* **29**, 205-211.

Tingdahl, K.M. and de Rooij, M. 2005. Semi-automatic detection of faults in 3D seismic data. *Geophysical Prospecting* **53**, 533-542.

Tryggvason, A. and Bergman, B. 2006. A travel time reciprocity discrepancy in the Podvin & Lecomte time3d finite difference algorithm. *Geophysical Journal International* **165**, 432–435.

Tryggvason, A., Rognvaldsson, S.Th. and Flovenz, O.G. 2002. Three-dimensional imaging of the P- and S-wave velocity structure and earthquake locations beneath Southwest Iceland. *Geophysical Journal International* **151**, 848-866.

Vidale. J. 1988. Finite-difference calculation of travel times. *Bulletin of the Seismological Society of America* **78**, 2062-2076.

Wildenborg, T. and Lokhorst, A. 2005. Introduction on CO_2 geological storage classification of storage options. *Oil & Gas Science and Technology- Rev. IFP* **60**, 513-515.